Chemosphere 273 (2021) 129550

Contents lists available at ScienceDirect

Chemosphere

journal homepage: www.elsevier.com/locate/chemosphere

Fate of radium on the discharge of oil and gas produced water to the marine environment

Faraaz Ahmad [a], Katherine Morris [a], Gareth T.W. Law [b], Kevin G. Taylor [a], Samuel Shaw [a, *]

[a] Research Centre for Radwaste Disposal and Williamson Research Centre, Department of Earth & Environmental Sciences, Williamson Building, The University of Manchester, M13 9PL, United Kingdom
[b] Radiochemistry Unit, Department of Chemistry, University of Helsinki, 00014, Finland

HIGHLIGHTS

- Selected field marine sediments in the vicinity of a wastewater discharge site contained elevated levels of Ra and Ba.
- Ra speciation and fate was determined via heavy liquid extractions, mixing experiments and geochemical modelling.
- Barite particles isolated from field sediments contained measurable ^{226}Ra activity confirming the radiobarite fate pathway.
- Synthetic/field produced waters were mixed with seawaters to successfully mimick the formation of (radio)barite particles.
- Ra uptake experiments showed Ra primarily exists in the form of radiostrontiobarite following produced water discharge.

ARTICLE INFO

Article history:
Received 1 September 2020
Received in revised form
19 December 2020
Accepted 1 January 2021
Available online 6 January 2021

Handling Editor: Martine Leermakers

Keywords:
Radium
Produced water
Precipitation
Barite
Offshore discharges
NORM

ABSTRACT

Understanding the speciation and fate of radium during operational discharge from the offshore oil and gas industry into the marine environment is important in assessing its long term environmental impact. In the current work, ^{226}Ra concentrations in marine sediments contaminated by produced water discharge from a site in the UK were analysed using gamma spectroscopy. Radium was present in field samples (0.1–0.3 Bq g^{-1}) within International Atomic Energy Agency activity thresholds and was found to be primarily associated with micron sized radiobarite particles ($\leq$2 μm). Experimental studies of synthetic/field produced water and seawater mixing under laboratory conditions showed that a significant proportion of radium (up to 97%) co-precipitated with barite confirming the radiobarite fate pathway. The results showed that produced water discharge into the marine environment results in the formation of radiobarite particles which incorporate a significant portion of radium and can be deposited in marine sediments.

1. Introduction

The presence of radionuclides, such as ^{226}Ra and ^{228}Ra, from the decay of naturally occurring ^{238}U and ^{232}Th have been detected in produced water effluents from oil and gas platforms across the world (Fisher, 1998; Røe Utvik, 1999). During extraction and production of oil and gas, radionuclides can be transported from the subsurface to the produced waters, dependent upon the chemical conditions of the reservoir (IOGP, 2016). Discharges of offshore effluents can then result in the release of these naturally occurring radionuclides such as ^{226}Ra and ^{228}Ra into the marine environment (Holdway, 2002; Grung et al., 2009; Dowdall and Lepland., 2012; Bakke et al., 2013). In addition, the release of produced water into the marine environment can result in the formation of inorganic particles e.g. barite ($BaSO_4$) due to the mixing of incompatible waters (i.e. produced water and seawater, Zhang et al., 2014). These particles can contain radium (e.g. ^{226}Ra) due to the ability of this radionuclide to co-precipitate into binary e.g. celestine ($SrSO_4$) and barite ($BaSO_4$), and ternary phases e.g. strontiobarite ($BaSrSO_4$) (Al-Masri and Aba., 2005; Rosenberg et al., 2014; Zhang et al., 2014). Naturally occuring radioactive material (NORM) is one of the regulated risks that have to be accounted for in some jurisdictions, such as the North Sea where the total discharge is monitored. There

* Corresponding author.
E-mail address: sam.shaw@manchester.ac.uk (S. Shaw).

https://doi.org/10.1016/j.chemosphere.2021.129550
0045-6535/

are many local and international regulations regarding onshore and offshore oil field emissions including; OSPAR (Oslo and Paris) Commission for EU (European Union) member states, DEFRA (UK Department for Environment, Food and Rural Affairs), the UK Environmental Agency (EA) and the UK Oil and Gas Authority (OGA), which oversees industry compliance with European Union (EU) regulations. However, the International Atomic Energy Agency (IAEA) in agreement with the International Commission on Radiological Protection (ICRP) and European Commission, explicitly define NORM as any natural radioactive material containing radionuclides in the uranium and thorium decay series with an activity concentration above 1 Bq g^{-1} (IAEA, 2004; ICRP, 2007; European Commision, 2014). To further predict the environmental fate of radium from produced waters it is critical to gain an understanding of radionuclide behaviour during the particle formation processes and nature of the material which forms upon discharge of produced water into the marine environment. This will help to underpin assessments of the environmental risk and fate of radium in these marine systems.

Oil and gas reservoirs in the subsurface typically also contain formation water. Formation water is transported to the surface with crude oil, natural gas, and sometimes sea water, during extraction as a complex mixture (Hunt, 1979; Holdway, 2002; Jerez Vegueria et al., 2002). This mixture subsequently undergoes industrial separation that leads to the creation of produced water, the largest waste effluent stream in the petroleum industry (Grung et al., 2009). The chemical and physical compositions of produced waters differ due to factors such as differing reservoir geology and the stage of oil and gas production. Produced waters are comprised of dissolved cations (Na^+, K^+, Ca^{2+}, Mg^{2+}, Ba^{2+}, Sr^{2+}), anions (SO_4^{2-}, Cl^-, HCO_3^-, CO_3^{2-}), and dissolved gases. The concentration of salts varies from a few mg L^{-1} up to $\geq$300,000 mg L^{-1} (Jacobs et al., 1992; Røe Utvik, 1999; Fakhru'l-Razi et al., 2009; Zhang et al., 2014). Isotopes of radium (^{224}Ra, ^{226}Ra and ^{228}Ra) and lead (^{210}Pb) are also present in produced waters due to leaching of primordial radionuclides (uranium and thorium) from the reservoir rock, which leads to their mobilisation to porewaters and resulting detection at a range of offshore installations around the world (Doyi et al., 2016). The naturally occurring radioactive nuclides of primary concern in oil and gas production are ^{226}Ra (half-life 1600 years) and ^{228}Ra (half-life 5.8 years). These decay into various radioactive progeny, before becoming stable lead. ^{226}Ra belongs to the ^{238}U decay series and ^{228}Ra to the ^{232} Th day series (IOGP, 2016). The level of NORM accumulation in oil and gas waste can vary substantially from one facility to another depending on reservoirs source geology and operational conditions and will also change over the lifetime of an oil producing well (IOGP, 2016).

As a result of temperature and pressure conditions altering during oil and gas extraction, carbonate and sulphate scales may deposit on the inside surfaces of production equipment. Scale formation can also occur during the injection of seawater to maintain reservoir pressure in the formation (Todd and Yuan, 1990; Yuan et al., 1994; Al-Masri and Aba., 2005; Badr et al., 2008; Garner et al., 2015). The tendency of radium to incorporate into insoluble barium and strontium sulphate mineral phases via co-precipitation results in the formation of NORM. This NORM forms as $Ra_xBa_{1-x}SO_4$ (radiobarite) and/or $Ba_xSr_yRa_zSO_4$ (radiostrontiobarite) due to the similar ionic radii of key ions (Ba: 1.61 Å, Ra: 1.7 Å, and Sr: 1.44 Å) in solution (Garner et al., 2015; Doyi et al., 2016). The dominant formation mechanism of these radium-containing scales is the mixing of chemically incompatible waters and establishment of supersaturated solutions during oil extraction operations where fluids, primarily sea water, interact with produced water and precipitation occurs. When sea water containing high sulphate (SO_4^{2-}) is mixed with produced water with low sulphate and high divalent cation concentrations alongside radium and radium series radionuclides, precipitation of radium-containing sulphate particles follows, and water with lower radioactivity (compared to the initial water) is subsequently produced (Candeias et al., 2014). Permitted discharge of produced water effluent to the marine environment therefore may drive the precipitation of sulphate particles, via the mixing of incompatible waters. This may lead to the uptake of radium into sulphate particles and/or the sequestration of radium via adsorption to existing particulates in the water column and/or sediment (Neff, 2002; Fakhru'l-Razi et al., 2009; Grung et al., 2009). There is uncertainty about the nature of these interactions and the speciation of radium during mixing of these waters. Understanding the speciation and fate of radium during operational discharges of production waters from the offshore oil and gas industry into the marine environment is essential in underpinning predictions of the fate of ^{226}Ra in these systems and further defining its overall environmental impact. Radium scavenging mechanisms such as adsorption, precipitation, and aqueous dispersion are fundamental processes affecting the mobility and fate of radium. Overall, it is expected that the formation of inorganic micro-particulate radiostrontiobarite ($RaBaSrSO_4$) ternary phases during production water/seawater mixing, via the mechanism of co-precipitation is a major pathway controlling ^{226}Ra fate in these systems, but there is a paucity of direct experimental evidence for this process (Gafvert et al., 2007).

Studies show the activity of radium discharged from production sites can be significant, with levels up to 1200 Bq L^{-1} reported across different installations (IOGP, 2016). Dowdall and Lepland. (2012) reported that discharges from Norwegian sites are typically of the order of 306–480 $\times$ 10^9 Bq y^{-1} with an average radium activity concentration of 3.3 Bq L^{-1}. Eriksen et al. (2006) showed that the concentration of ^{226}Ra discharged from North Sea platforms is up to 21 Bq L^{-1} and is consistent with American platforms where 37 Bq L^{-1} have been recorded (Eriksen et al., 2006; Olsvik et al., 2012; Bakke et al., 2013; Pardue and Guo, 1998). Jerez Vegueria et al. (2002) showed offshore discharges from platforms in Brazil are on the order of 2–30 m^3 d^{-1} with a varying ^{226}Ra concentration between 0.012 and 6 Bq L^{-1} (Jerez Vegueria et al., 2002). These studies illustrate discharge volumes and levels of activity vary considerably globally. Background radium concentrations within surrounding seawaters are typically around three orders of magnitude lower than those in produced waters (e.g. 0.01–0.03 Bq L^{-1}) (Jerez Vegueria et al., 2002; Gafvert et al., 2007; Dowdall and Lepland., 2012). This suggests that discharge of produced waters provides a significant point source for radium.

In terms of dilution and dispersion, research by Jerez Vegueria et al. (2002) revealed the lack of significant radium contamination within sediment or seawater samples around platforms as a result of dispersive effects by currents (Jerez Vegueria et al., 2002). In contrast, possible accumulation of radiobarite has been identified in other studies, inferring that under certain conditions, discharge of effluents may result in radiobarite precipitation and subsequent sedimentation. For example, Pardue and Guo. (1998) identified contaminated oilfield sediment samples contained barite from bulk analysis, and demonstrated correlations between radium and barite suggesting radium solubility was most likely controlled by its co-precipitation with barite. However, to date, NORM particles have not been extracted and directly characterised to provide evidence of radiobarite in either experimental or field-based studies (Pardue and Guo., 1998). Indeed, variable findings from different study sites suggests that the setting and physicochemical characteristics (e.g. water depth, salinity, current flow and mineralogical distribution) of the receiving environments is key to controlling the mechanisms of radium interactions in estuarine and marine settings (Landa and Reid, 1983; Pardue and Guo., 1998;

Gafvert et al., 2007; Van Sice et al., 2018; McDevitt et al., 2019).

The co-precipitation of radium in barite has been studied experimentally in relation to produced water discharges and in uranium mining (Doerner and Hoskins., 1925; Gordon and Rowley., 1957; Beneš et al., 1981; Fedorak et al., 1986; Jerez Vegueria et al., 2002; Rosenberg et al., 2011(b), 2014; Zhang et al., 2014). Results show that radium removal via co-precipitation into binary (Ra-$BaSO_4$ or Ra-$SrSO_4$) or ternary phases (Ra-$BaSrSO_4$) is controlled by the ionic strength of the solution and the nucleation kinetics of the barite-containing particles (Rosenberg et al., 2011a, 2011b). The distribution coefficient has been widely adopted to empirically describe radium co-precipitation in barite using the radium and barium concentration ratios in the aqueous and solid phases. This is known as the concentration-based effective partition coefficient (Equation 1).

$$K'_{D,barite} = \frac{(dRa/dBa_{solid})}{([Ra]/[Ba]_{solution})}$$

Equation 1: Concentration-based effective partition coefficient (K'_D); [*Ra/Ba*] represents the aqueous concentration of the element, and *d*Ra/Ba_{solid} represents the concentration of the element in the solid (e.g. Ra or Ba) (Rosenberg et al., 2014).

Experimental partition coefficients reported in simple systems range between 1.07 and 1.54 in dilute solutions (ionic strength: 0 M) and up to 7.49 (ionic strength: 3 M) (Rosenberg et al., 2014; Zhang et al., 2014). To date work on the co-precipitation of radium during barium uptake has been based on simple synthetic solutions rather than field samples or full-component brines. This means that the formation process, composition (e.g. Ra_{solid} concentration) and morphology of the barite NORM which is produced during discharge to the marine environment is poorly constrained under field relevant environmental conditions.

In this study, firstly we explored the uptake and fate of radium in sediment samples obtained from a field site where produced waters are discharged into the marine environment. The bulk field sediment samples were assessed using gamma spectroscopy, X-ray diffraction (XRD), and X-ray fluorescence (XRF). In addition, heavy liquid extractions were used to separate radiobarite particles from marine sediments, and to further characterise their bulk chemistry, morphology/particle size (scanning electron microscopy, SEM) and radioactivity (autoradiography). Secondly, we extend these observations to experimental systems where both synthetic (full-component) and field derived produced waters were mixed with synthetic and field derived seawaters to further quantify the formation process of radiobarite particles in marine discharge relevant environmental conditions. By combining field and laboratory-based observations we were able to further define the fate of radium (^{226}Ra) within produced water when discharged into the marine environment. To the best of our knowledge this is the first paper to extract, assess and fully characterise the precipitate which forms from the discharge of produced water to seawater using both natural and synthetic waters providing a better understanding of the mechanism of formation and helping to predict the fate of radium (^{226}Ra) in these systems.

2. Materials and methods

2.1. The study area and experimental method

2.1.1. Marine sediment

Marine sediment samples were collected in April 2017 close to a near-shore produced water discharge point. A total of 5 samples (A - E) were taken at different distances from the outfall (20–250 m) (Fig. 1). Seabed sediment (10–15 cm) was collected using a Day grab

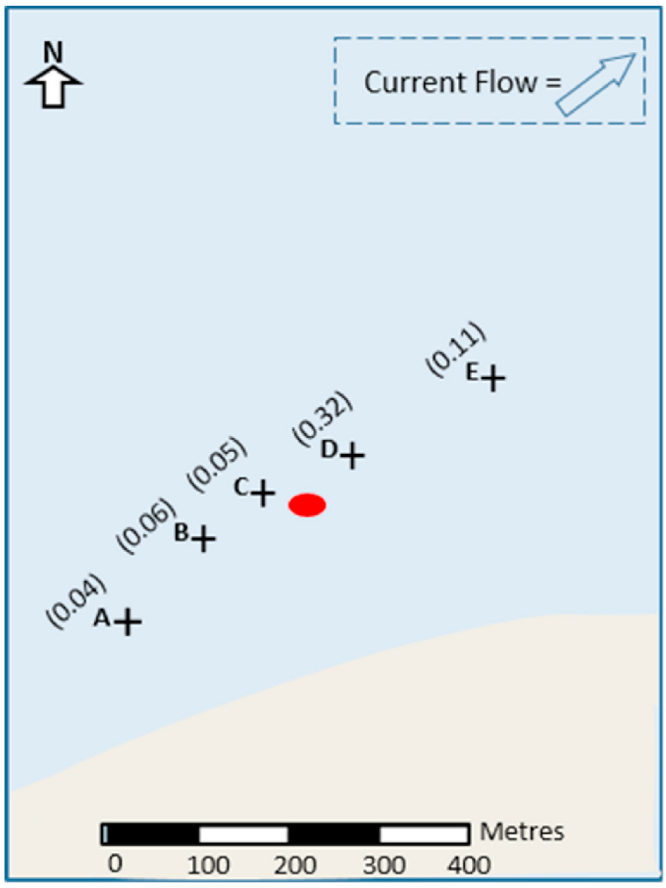

Fig. 1. Schematic showing sample (A–E) locations relative to the discharge outfall (red marker), recorded radioactivty (Bq g^{-1}) and current flow direction. (For interpretation of the references to colour in this figure legend, the reader is referred to the Web version of this article.)

(0.1 m^2) and were placed in sterile bags in an ice box to maintain the redox conditions during transport. Samples were stored at 4 °C and prior to characterisation, they were homogenised and dried.

2.1.2. Produced water and seawater mixing experiments

Produced water from an active oil field in the North Sea and seawater from Formby Beach in Merseyside, UK were obtained using acid washed and rinsed Nalgene carboys and stored at 4 °C prior to use. These locations are in the same global region. Synthetic North Sea seawater and produced water compositions were also made up (Table 2) (Todd and Yuan, 1992). Both field and synthetic seawaters and produced waters were mixed in large scale (4.5 L) precipitation experiments in a 9:1 ratio to mimic the discharge of produced water into a large body of seawater. They were then stirred (180 rpm) for 24 h prior to further analysis. This was followed by filtration (≤0.22 μm PES filter) and drying (40 °C ± 0.5 °C) to harvest the resultant precipitates for characterisation. Modelling with PHREEQC 3.3.9 using the S.I.T. database coupled to geochemical data for the seawaters and produced waters was used to calculate the saturation index of the solid phase (e.g. barite) for these experimental systems.

2.1.3. Radium uptake experiments

A synthetic produced water stock solution (Table 2) was spiked with ^{226}Ra (100 Bq mL^{-1} from a 10 kBq pH 3 HCl stock) and the pH was readjusted with dilute KOH solution. Small scale (1.5 mL) synthetic seawater and spiked synthetic produced water

experiments were conducted by mixing the solution in a 9:1 seawater to produced water ratio. The samples were continuously mixed (180 rpm) for 7 h with periodic sampling and samples were run in series to allow sacrificial sampling. At each time point, samples were centrifuged at 14800 rpm for 5 min and aqueous radium concentrations were determined by adding 1 mL of the centrifuged solution to 10 mL of scintillation cocktail (Ultima Gold) in a sealed tube and stored in the dark prior to analysis. Samples were then analysed in a Quantalus scintillation counter (PerkinElmer) after 1 month dark storage to allow short-lived radon progeny to equilibrate (Siddeeg et al., 2015). Parallel, inactive experiments were run to allow cation and anion analysis using Inductively Coupled Plasma Atomic Emission Spectroscopy (ICP-AES, PerkinElmer Optima 5300 DV) and Ion Chromatography (IC, Dionex ICS 5000).

2.2. Analytical methods

2.2.1. Solid phase characterisation

XRD (Bruker D8 Advance diffractometer) and XRF (PANalytical Axios) were used to determine the bulk mineralogical and chemical compositions of inactive precipitates and sediment samples. The sediment was dried in an oven (40 °C ± 0.5 °C), disaggregated using a pestle and mortar and homogenised in an agate ball mill to a fine consistency for XRD and XRF analysis. The organic matter content of the sediments was estimated from loss on ignition at 110–1000 °C for 2 h (Table S1) (Siddeeg et al., 2015). Sediment samples were also dried at (50 °C ± 0.5 °C) to calculate the moisture content and dry sediment weight (Table S1). Fourier-transform infrared spectroscopy (PerkinElmer Spotlight 400 FTIR imaging system Universal ATR) was used to characterise the inactive precipitate obtained from parallel inactive mixing experiments. Brunauer- Emmett – Teller (BET) surface area analysis of the inactive precipitates was also performed (Micromeritics Gemini V Surface Area Analyser 2365). The molar stoichiometry of the strontiobarite precipitates formed from larger mixing experiments (4.5 L seawaters: 0.5 L produced waters) was determined by dissolution into pH 13 EDTA to dissolve barite and the Sr and Ba concentrations were then measured using ICP-AES (Averyt et al., 2003). A FEI QUANTA 650 FEG ESEM (Field Emission Gun, Environmental Scanning Electron Microscope) equipped with Bruker Quantaz Energy Dispersive Spectroscopy system with an XFlash detector was used for imaging and analysis of the chemical composition of both inactive precipitates and particles separated from sediments samples using heavy liquid extraction. The backscattered electron (BSE) detector was used to image the samples and allow atomic number contrast analysis. EDS was used to assess the chemistry of the samples. The speciation of strontium associated with barite was further analysed via X-ray absorption spectroscopy (XAS). A sample (approximately 2 wt % Sr) was mounted in a cryo vial and analysed at Diamond Light Source, Harwell, UK on beam-line B18. Sr K-edge spectra were collected in transmission mode at 77 K. Background subtraction and improvement of signal to noise ratio of the data was obtained by averaging multiple scans for the sample using the Demeter software package Athena and Artemis, FEFF6 (Ravel and Newville., 2005).

2.2.2. Radiometric analysis

Radium activities in the sediments and produced waters were measured using gamma spectroscopy (Ge(Li) Canberra) with a high purity germanium detector (HPGe). To avoid the escape of radon gas, the samples were sealed in a double propylene container and put aside for 1 month to reach secular equilibrium. The counting equipment was calibrated using matrix-matched standards spiked with certified standard solutions of ^{226}Ra. A^{226}Ra labelled sediment standard (200 Bq in 50 g) for gamma spectroscopy counting was prepared as per method of Siddeeg et al. (2015). For produced water measurements standards were made by adding aqueous ^{226}Ra spike to synthetic produced water (2500 Bq in 500 mL) in a polypropylene container and sealing for one month prior to analysis. The samples were counted for 24 h (sediment) or 7 days (produced water) and the radium activities were calculated from measurements of the ^{214}Bi and ^{214}Pb daughter products and comparing these to known standards (Siddeeg et al., 2015). Errors were calculated using the standard deviation and error propagation (Table S2) (Siddeeg et al., 2015).

2.2.3. Heavy liquid extraction

Oven dried sediments were disaggregated and sieved to < 215 μm. Heavy liquid (di-iodomethane; 3.3 g cm^{-3}) was then used to separate the barite-containing (4.5 g cm^{-3}) dense fraction of the sediment. An accurately weighed, sieved solid sample between 10 and 20 g was added to a separating funnel containing 80 mL heavy liquid and left to separate for 10 min. Both the dense fraction (>3.3 g cm^{-3}) and light fraction (<3.3 g cm^{-3}) were then separated and filtered. Both fractions were then rinsed with deionised water, then acetone, and dried. The samples were then examined under a light microscope and white barite like particles were handpicked for further SEM analysis.

2.2.4. Autoradiography

Autoradiography was used to determine the spatial distribution of radioactivity in selected samples from the field study site. Handpicked barite like samples were placed on a storage phosphor screen (BAS-IP SR, super resolution: G.E Healthcare) in a dark cupboard for 4 weeks. The plate was then imaged using a Typhoon 9410 variable mode imager where the screen was then scanned and imaged using a HeNe laser (633 nm) with a pixel size resolution of 10–25 μm. The extent of darkening recorded is quantitatively proportional to the activity on the sample surface (Zeissler et al., 2001).

3. Results & discussion

3.1. Formation of radiobarite precipitate upon discharge of produced water to a marine system: field study

3.1.1. Characteristics of marine sediment samples

The bulk mineralogical composition of the five sediment samples were dominated by silicate minerals such as quartz (SiO_2), mica (muscovite; $KAl_3Si_3O_{10}(OH)_2$), feldspar (albite; $NaAlSi_3O_8$), and chlorite (clinochlore; $(Mg,Fe,Al)_3(Al,Si)_4O_{10}(OH)_8$). All samples contained carbonate minerals (aragonite and calcite; $CaCO_3$) and halite (NaCl). Three samples contained kaolinite ($Al_4(SiO_{10})(OH)_8$), ankerite ($Ca(Fe,Mg,Mn)(CO_3)_2$), or microcline ($KAlSi_3O_8$) (Table 1). The compositions of the sediments as measured by XRF are shown in Tables S3–4. The concentrations of Ba and Sr in the sediment are summarised in Table 1.

The ^{226}Ra content of the samples ranged from background levels (0.04–0.06 Bq g^{-1}) to 0.32 Bq g^{-1}. Here there was a spatial trend with samples west of the discharge outfall (A – C; Table 1) that are near background, and samples east of the outfall (D and E; Table 1) that are elevated above background (0.1 and 0.3 Bq g^{-1}). Interestingly, the elevated Ra concentration was well correlated with the Ba concentration in sample D (Table 1) as supported by further characterisation (see below). This confirms co-enrichment of Ra within Ba bearing sediments presumptively due to Ra incorporation into barite (Jerez Vegueria et al., 2002; Rosenberg et al., 2014; Zhang et al., 2014; Garner et al., 2015). The variation in spatial distribution of radium is presumably due to current dispersion effects as

Table 1
Mineralogical, radiological and chemical characteristics of the sediment samples (A-E) collected from the disacharge outfall. W = west from outfall, E = east from outfall. Typical error for XRF analysis are ± 5%.

Sediment Sample	Mineralogy	Chemical Composition		Radioactivity
		Sr (ppm)	Ba (ppm)	^{226}Ra (Bq g^{-1})
A: 250 m W	Quartz, Muscovite, Albite, Clinochlore, Calcite, Aragonite, Halite	870	241	0.045 ± 0.004
B: 100 m W	Quartz, Analcime, Muscovite, Albite, Microline, Clinochlore, Kaolinite Calcite, Aragonite, Ankerite, Halite	558	370	0.06 ± 0.01
C: 20 m W	Quartz, Muscovite, Albite, Clinochlore, Calcite, Aragonite, Halite	375	310	0.05 ± 0.01
D: 100 m E	Quartz, Muscovite, Albite, Microline, Clinochlore, Kaolinite, Calcite, Aragonite, Halite	552	1180	0.32 ± 0.05
E: 250 m E	Quartz, Muscovite, Albite, Microline, Clinochlore, Kaolinite Calcite, Aragonite, Ankerite, Halite	252	345	1.11 ± 0.01

there is a north-east flow direction at the site indicating deposition of Ba and Ra in the sediment with enrichment to the east (Fig. 1). The lack of correlation between the Ra and Ba concentrations in sample E in comparison to sample D is presumably due to a proportion of radium that may not co-precipitate with barite once discharged, instead adsorbing to sediment and particulates down current of the wastewater discharge due to tidal flow effects (Landa and Reid., 1983; Van Sice et al., 2018; McDevitt et al., 2019). As discussed above, samples A – C are at background Ra concentrations (0.01–0.05 Bq g^{-1}) found within marine sediments (Landa and Reid, 1983; Jerez Vegueria et al., 2002; Hosseini et al., 2010; Dowdall and Lepland, 2012; Environment Agency, 2015). The Ba and Sr levels are also relatively low compared to D but similar to E (approximately 300 ppm) which again are background concentrations in marine sediments (Stevenson et al., 1995; Jerez Vegueria et al., 2002). Interestingly, Sr levels in sample A were higher than expected presumably due to higher proportions of diagenetic minerals (i.e. carbonates and clays) (Schlanger, 1988). For samples D and somewhat E the Ra levels are elevated compared to background and this coincides with higher Ba levels in the sample and/or tidal flow effects (Table 1). This suggests sample D has technologically enhanced levels of Ra that is co-associated with barite in the sediment with a small radiological enhancement in the vicinity due to possible adsorption of Ra to the surface of sediments, presumably due to the produced water discharge.

Further analysis of the mineralogy of the sediment was performed to explore the relationship between Ra and Ba observed at bulk levels. Here, heavy liquid separation allowed isolation of the dense mineral fraction in sample D. The isolated grains (>3.3 g cm^{-3}) were typically 240–430 μm irregular aggregates, which consisted of individual equant particles ≤ 2 μm in size (Fig. 2). EDS spectra and elemental mapping showed that the particles were rich in Ba, Sr, and S consistent with strontiobarite compositions. In addition, certain areas were abundant in Al, Ca, and Si, presumably due to the presence of silicate particles, for example clays (Fig. 2).

Select isolated agglomerates of strontiobarite were analysed using autoradiography where it was clear that the particles contained measurable radioactivity most likely corresponding to radium (^{226}Ra) and consistent with the gamma spectroscopy data for bulk sediment samples (Table 1,Fig. 2 and S1-2). Overall, these results indicate that marine sediment samples east of the discharge outfall contained enhanced levels of Ba and Ra as a result of radiostrontiobarite co-precipitation and deposition.

The sediments that contained elevated levels of radium (^{226}Ra) also showed evidence of microbially-mediated reducing conditions at the collection sites (Fig. 3, Folk, 2005). EDS spectra on bulk samples (i.e. sample D) highlighted the presence of particles that were rich in Fe and S, which is indicative of pyrite (FeS_2), Ba and Sr indicative of strontiobarite, and Al, Mg and Si indicative of silicate particles (Fig. 3b). The size of the pyrite grains (<10 μm) and morphology (framboidal) indicates this pyrite has formed in mildly sub-oxic to sulfidic waters (Roychoudhury et al., 2003). Roychoudhury et al. (2003) and Proske et al. (2015) have shown that the formation of framboidal pyrite in marine sediments is due to the redox conditions below the sediment-water interface, where microbial activity results in the consumption of organic matter during sulphate-reduction and the formation of framboidal pyrite (Fig. 3). This suggests a robust microbial community and highly reducing environment as expected in near-shore marine sediments (Roychoudhury et al., 2003; Folk, 2005; Proske et al., 2015).

Interestingly, this indicates that sulphate-reduction is occurring within the sediment in which barite is deposited. Microbial induced sulphate-reduction causes a decrease in sulphate which may induce barite dissolution as shown from previous studies (Pardue and Guo., 1998; VanLoon, 2000; Phillips et al., 2001; Keith-Roach, 2002; Ouyang et al., 2017). Bioreduction processes stimulated in natural sediment systems including Fe(III)-reduction and sulphate-reduction, have been suggested as possible mechanisms for remobilisation and increased solubility of radium from radiobarite. (Fedorak et al., 1986; Pardue and Guo., 1998; Phillips et al., 2001). Whilst there have been studies on terrestrial discharges of radium in engineered and natural settings (Bolze et al., 1974; Fedorak et al., 1986; Baldi et al., 1996; Phillips et al., 2001; Wilkins et al., 2007; Luptáková et al., 2015; Ouyang et al., 2017), there are limited studies that focus upon marine discharges of oil produced water (Pardue and Guo, 1998). This suggests that the long-term environmental fate of radiobarite as biological processes and reducing conditions develop merits further investigation.

3.2. Strontiobarite formation during field and synthetic seawater and produced water mixing: morphology and composition

3.2.1. Field mixing experiments

To further investigate strontiobarite precipitation, produced water mixing experiments were conducted using the field produced water sample and representative seawater sampled from the near-shore (Table 2). Gamma spectroscopy analysis of the field produced water indicated non-detectable radium. Produced water and seawater were mixed in a 1:9 ratio which resulted in the formation of a white precipitate. After separation, SEM analysis revealed mineral grains with an equant morphology (Fig. 4a).

EDX analysis showed that the composition of the precipitate was consistent with strontiobarite (Fig. 4b). Here, particle size distribution determined by SEM was between 1 and 6 μm, typical of natural barite found in sediment (Phillips et al., 2001; Gonneea and Paytan., 2006). Aqueous analysis of the experimental solutions before and after mixing, showed the composition of the precipitate was ($Ba_{73.1}Sr_{26.3}SO_4$) (Table S5), which is consistent with strontiobarite (Todd and Yuan, 1990, 1992). Further analysis of the composition of the precipitate using XRD and EDTA dissolution was not possible as the mass of the precipitate produced was very small (see below). Other minor phases such as sodium chloride (NaCl) and magnesium sulphate ($MgSO_4$) were also identified in the SEM.

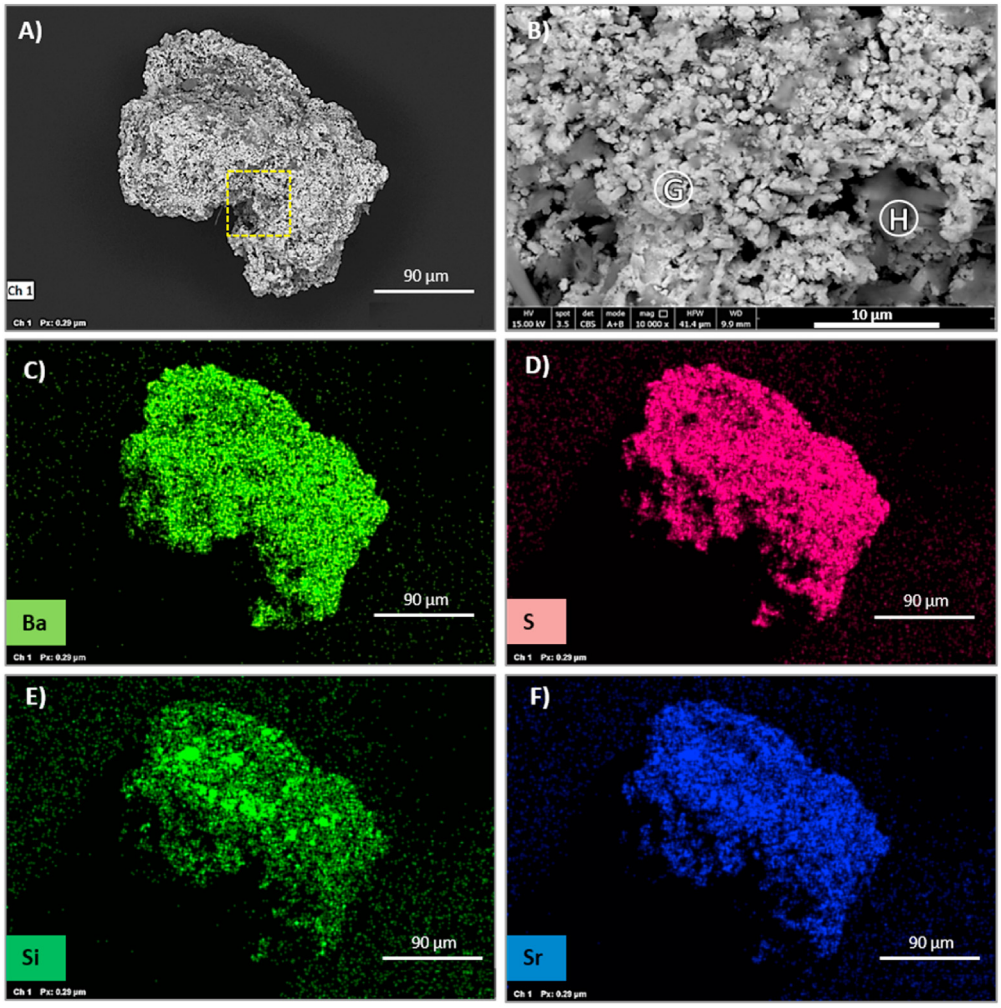
A)
90 µm
Ch 1
B)
G
H
10 µm
C)
Ba
90 µm
D)
S
90 µm
E)
Si
90 µm
F)
Sr
90 µm

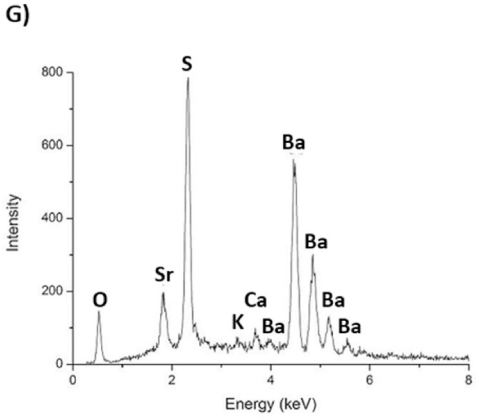
G)
Intensity
Energy (keV)
O
Sr
S
Ca
K
Ba
Ba
Ba
Ba
Ba

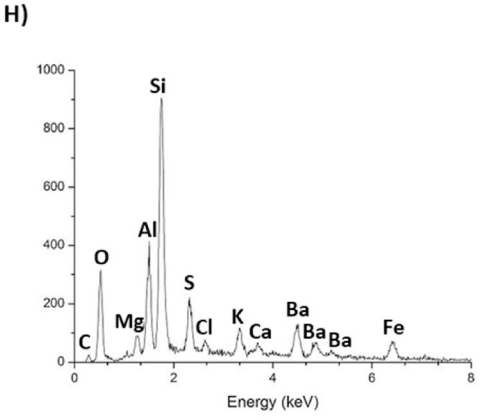
H)
Energy (keV)
C
O
Mg
Al
Si
S
Cl
K
Ca
Ba
Ba
Ba
Fe

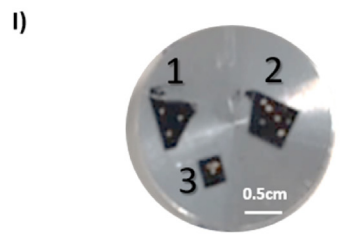
I)
1
2
3
0.5cm

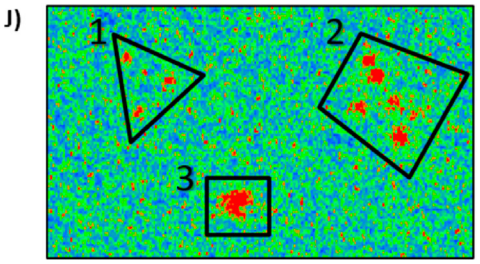
J)
1
2
3

Overall, mixing of field production water and seawater produced strontiobarite particles 1–6 μm in diameter. These were consistent with the individual strontiobarite particles separated from the field sediment samples using heavy liquid extraction (Fig. 2).

3.2.2. Synthetic mixing experiments

As well as the field production water and seawater sample experiment, we also performed mixing experiments with synthetic production water and seawater (Table 2) to further validate our results, methodology and approach, and to obtain enough precipitate for additional characterisation.

The synthetic produced waters and seawaters contained Ba and Sr at concentrations representative of those found in field brines from the North Sea (Mitchell et al., 1980; Yuan et al., 1994; Røe Utvik, 1999). After separation of the precipitate following the mixing of the waters (1 : 9 ratio), SEM analysis revealed mineral grains that exhibited an equant morphology (Fig. 5a). Here, the particle size distribution was between 1 and 5 μm. The mass of precipitate produced in these experiments was analysed using XRD confirming the precipitate was strontiobarite (Fig. S3). EDTA dissolution experiments further confirmed the composition of the precipitate to be $Ba_{76.4}Sr_{23.8}SO_4$ and consistent with that obtained from solution analysis before and after mixing ($Ba_{75.7}Sr_{24.3}SO_4$) (Table S5). Furthermore, EDX confirmed the precipitates contained Sr and Ba in similar ratios to the sediment samples and the field produced water and seawater mixing experiments. EDX analysis also indicated minor amounts of calcite were present in the sample (Fig. 5b). FTIR analysis of the precipitate showed intense peaks at 1084 cm^{-1} (with a distinct shoulder at 988 cm^{-1}) corresponding to the sulphur-oxygen (S–O) stretch and at 609 cm^{-1} (with a shoulder at 639 cm^{-1}) corresponding to the bending motion of the sulphur-oxygen bond within sulphate characteristic of barite (Fig. S4) (Adler and Kerr., 1965; Ramaswamy et al., 2010). Finally, the best fit to the Sr EXAFS data was consistent with Sr substituted within the structure of barite (Fig. S5). The coordination numbers and interatomic distances for Sr closely reflected the expected local environment of Ba^{2+} in pure barite (Fig. S5). The distance of the first Sr–O_1 shell (2.63 Å) in the sample was shorter than the Ba–O_1 (2.81 Å) distance in barite, consistent with the larger size of the Ba^{2+} (1.68 Å) ion compared to Sr^{2+} (1.48 Å) (Tokunaga et al., 2018). This confirms in these laboratory experiments, Sr^{2+} precipitates with barite and substitutes for Ba^{2+} into the crystal structure via co-precipitation consistent with past work (Hedström et al., 2013; Tokunaga et al., 2018).

Despite minor differences in the composition of the synthetic waters used in the experiments compared to the field waters, the composition and phase produced was consistent with the radiostrontiobarite extracted from marine sediment samples and field mixing experiments. Small differences in the crystal morphology and particle size across the different mixing experiments (e.g. rosette, equant), and other minor phases identified, maybe due to variations in the concentration of scaling ions (e.g. Sr^{2+} and Ba^{2+}) present in the produced waters and seawaters, and their resultant supersaturation in solution. This is shown by the saturation indices (SI) of mineral phases calculated via geochemical speciation modelling (PHREEQC) (Table 2). Overall this shows that the precipitate that forms from the synthetic fluids used to mimic the product produced in the field closely resembles those formed from field fluids, and matches chemically and morphologically to those found in field sediment. This laboratory based synthetic method can therefore be used to explore the uptake of Ra, and formation of the precipitate formed in the field in a marine setting (see section 3.3).

3.3. Radium uptake during strontiobarite (Ba–Sr–SO_4) formation

3.3.1. Synthetic seawater and produced water mixing

After confirmation that strontiobarite, with similar characteristics to those found in the field samples precipitated upon mixing of synthetic production waters and seawaters, further experiments were undertaken to investigate Ra uptake during this process. Experiments were performed to determine the distribution of Ra between the solid and aqueous phases following formation of the ternary phase ($RaBaSrSO_4$). The Sr, Ba, and Ra concentrations in solution with time are shown in Fig. 6a and b. After mixing, removal of Ba and Ra from solution occurred rapidly, presumably due to precipitation of radiostrontiobarite (Fig. 6a and b). This confirms rapid barite precipitation kinetics controls the uptake of Ra in this system. During the period of crystal growth (3–24 h) a portion of Ra is likely incorporated into the structure of the carrier mineral (i.e. barite) via direct substitution of Ra^{2+} for Ba^{2+} (Fig. 6a and b) (Zhang et al., 2014). After this period (24–1000 h) the activities of electrolytes and growth rate decreases (Fig. 6a and b) (Todd and Yuan., 1990; Zhang et al., 2014). As shown in Fig. 6a and b, Ra removal occurred coincident with Ba removal, and Sr removal occurred at a slower rate compared to Ba or Ra (Vinograd et al., 2018). Radium uptake increases over time, from 48% to 79% between 1 and 7 h, followed by a further increase up to 97% by 24 h. Equilibrium was then established with a maximum Ra uptake of 97.5%. An effective partition coefficient (Kd') for Ra^{2+} uptake into barite of 1.14 ± 0.1 was calculated, which agrees with results reported by other studies of 1.07–1.54 under similar ionic strengths (NaCl concentration: 0–3 M) (Ceccarello et al., 2004; Rosenberg et al., 2014; Zhang et al., 2014). Overall, this method effectively mimics the formation of precipitate in field samples (Section 3.2), and also produces uptake coefficients similar to those reported in literature for simple systems (Rosenberg et al., 2014; Zhang et al., 2014).

4. Conclusion and environmental implications

Elevated levels of ^{226}Ra were identified in field marine sediment samples (D and E) associated with radiostrontiobarite at sites hundreds of metres downstream from the point of produced water discharge. This suggested the produced water discharges may be associated with detectable and tolerable levels of radiation below IAEA threshold levels. Particles extracted from field marine sediments in this study show Ra is co-precipitated into strontiobarite. The mechanism of strontiobarite formation was further demonstrated from field and synthetic mixing experiments confirming the formation process. Micro-particulate strontiobarite precipitates with uniform composition, characteristic equant morphology, and particle size (1–6 μm), were identified in field samples and under different yet representative experimental regimes (e.g. field and synthetic mixing experiments), rather than a combination of barite and celestite.

This study of produced water discharges to the marine environment shows a direct link between the morphology and composition of the radiostrontiobarite precipitate extracted from field marine sediment samples, and the mixing of full-component

Fig. 2. (A–B), BSE images and elemental maps of the radiostrontiobarite particles extracted from marine sediment using heavy liqud extraction. Yellow box in (A) highlights area covered in (B); (C–F), corresponding elemental maps (Ba, S, Si and Sr respectively); (G), EDS spectra representative of the strontiobarite grains (bright regions) via point analysis (G); (H), EDS spectra representative of the clay rich areas (dark regions) via point analysis (H); (I), stub sample containing radiostontiobarite particles and; J) the corresponding autoradiograph. (For interpretation of the references to colour in this figure legend, the reader is referred to the Web version of this article.)

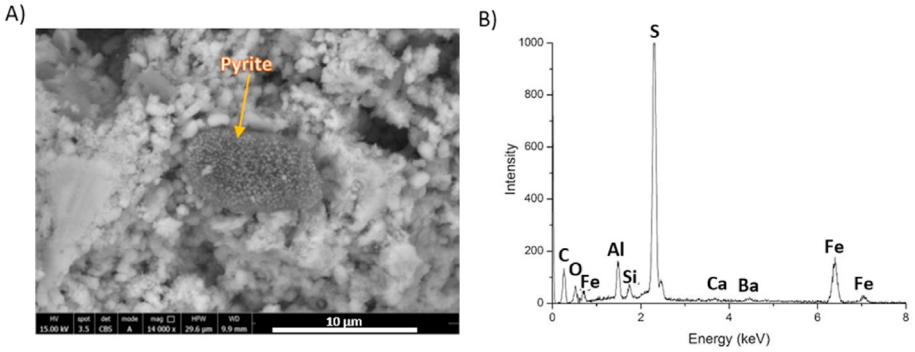

Fig. 3. (A) BSE image showing frambodial pyrtie crystals found in field sediment samples contaminatied with radiostrontiobarite and; (B) EDS spectra collected confirming the identificaation of pyrite.

Table 2
Field and synthetic seawater and produced water compositions (Todd and Yuan, 1992). Ionic strength and saturation index (SI) of mixtures calculated using PHREEQC modelling software with a 9:1 mixing ratio.

Ions	Produced water – field (mg L^{-1})	Seawater – field (mg L^{-1})	Produced water – synthetic (mg L^{-1})	Seawater – synthetic (mg L^{-1})
Ca	7860 ± 220	336 ± 8	2260 ± 41	420 ± 6
K	1840 ± 30	381 ± 61	380 ± 4	467 ± 4
Mg	4190 ± 100	972 ± 26	367 ± 9	1300 ± 18
Sr	323 ± 9	6 ± 1	537 ± 6	8 ± 0.1
Ba	13 ± 1	0.3 ± 0.3	209 ± 3	0
Na	80500 ± 1900	8290 ± 196	23900 ± 356	10100 ± 121
Cl	15700 ± 182	7690 ± 1710	50700 ± 68	19200 ± 268
SO_4	278 ± 8	838 ± 228	0	2930 ± 23
HCO_3	39	18 ± 0.5	0	111 ± 10
Initial pH	8.27 ± 0.13	8.13 ± 0.02	5.45 ± 0.08	8.12 ± 0.02
Initial Ionic Strength	2.69 M	0.41 M	1.38 M	0.62 M
Final Ionic Strength	0.64 M		0.69 M	
SI_{BaSO4}	1.22		2.94	

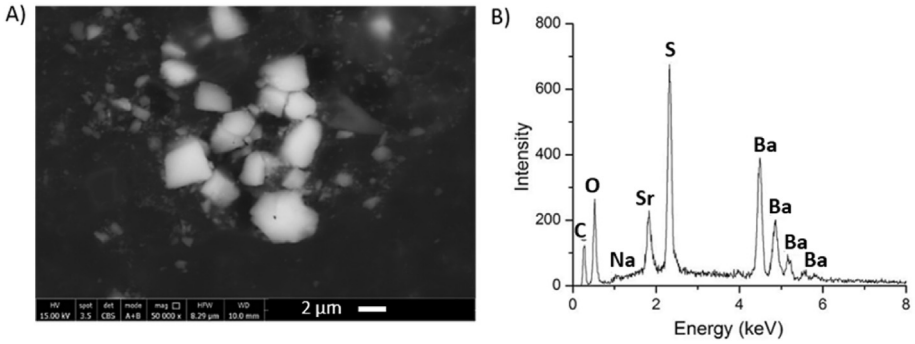

Fig. 4. (A) BSE image showing strontiobarite crystals exhibiting tabular morphology with a particle size ranging from 2 to 6 µm from field mixing experiments with field productions and seawater samples and; (B) EDS spectra representative of all grains.

synthetic and field produced waters and seawaters. Note that despite the differences in composition of the synthetic and field produced water (Table 2) the precipitated (radio)strontiobarite are similar in composition and morphology. This indicates that the formation of this phase is likely to be common to a broad range of produced water discharge scenarios. This compares well with other studies where related morphologies and compositions are seen for similar systems (e.g. water flooding studies) producing strontiobarite during the mixing of incompatible waters (Todd and Yuan., 1990, 1992).

Insight into radium solid-solution chemistry and radiostrontiobarite formation via this mechanism of mixing incompatible waters, as a result of operational discharges, can help to predict and model the fate and behaviour of ^{226}Ra marine systems. Radium uptake experiments show that a portion of radium (48–79%) is incorporated into strontiobarite between 1 and 7 h and >97% incorporation over 24 h, suggesting that on discharge some radium may well be dispersed into solution dependent upon the characteristics of the receiving environment. A value of 1.14 ± 0.1 was calculated for the effective partition coefficient (Kd') for Ra^{2+} incorporation into strontiobarite, which is comparable to other studies in this area investigating binary and ternary phases e.g. in fracking systems (or other controlled studies) under controlled conditions (Rosenberg et al., 2014; Zhang et al., 2014).

Results obtained in this study in respect to Ra uptake are representative of a closed-system, whereas marine discharges in

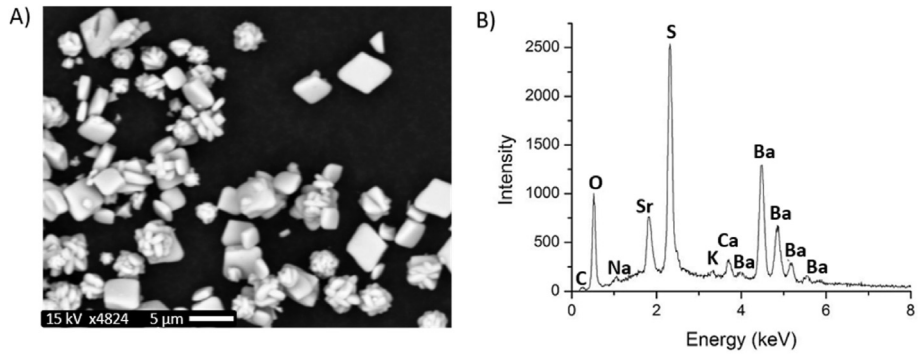

Fig. 5. (A) BSE image showing the strontiobarite crystals exhibiting both tabular and rosette morphology with a particle size between 1 and 5 μm and; (B) EDS spectra representative of all grains.

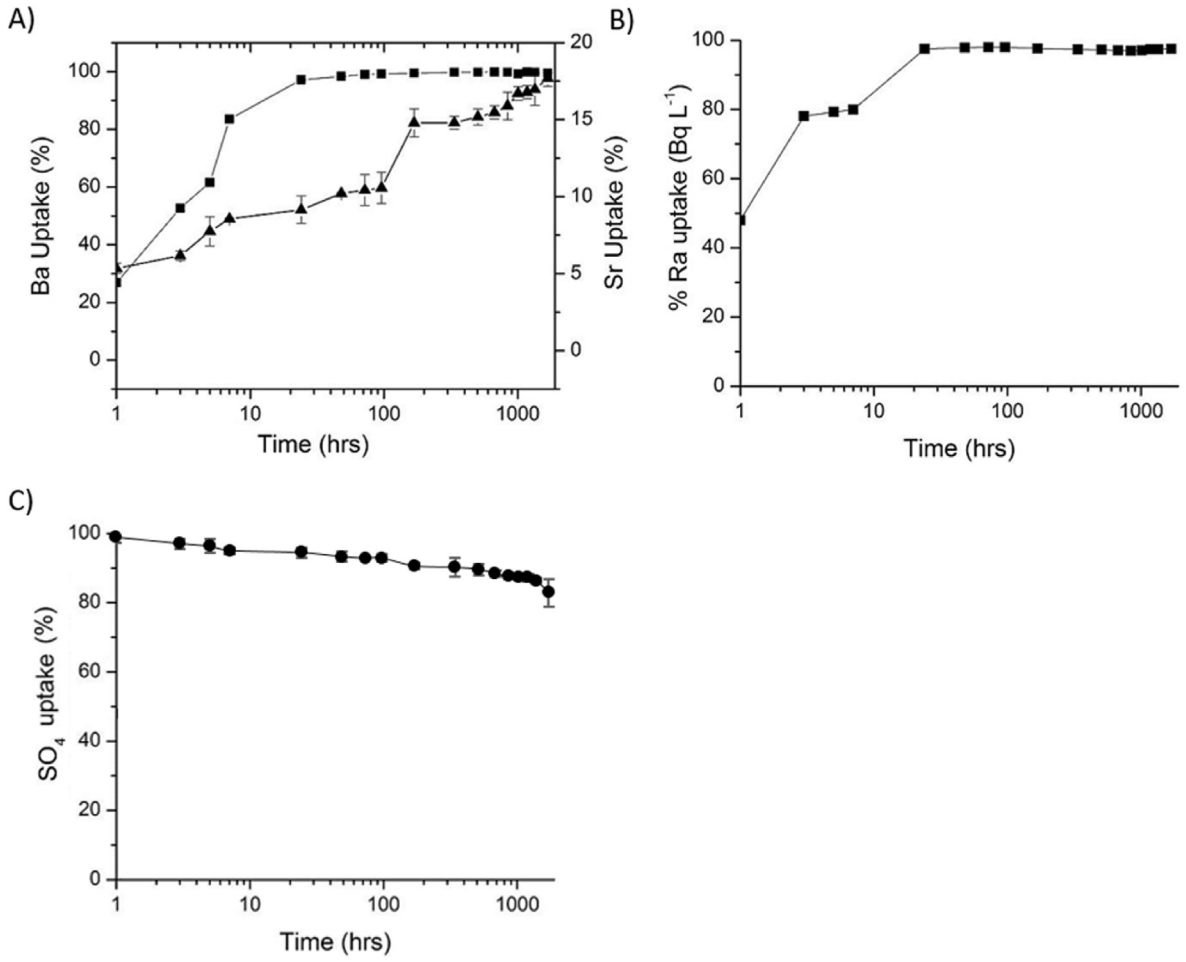

Fig. 6. A) Percentage uptake of Ba (■) and Sr (▲) over time (1.5 mL small scale experiments); B) ^{226}Ra uptake over time (■) (1.5 mL small scale experiment; initial activity 13Bq mL^{-1}) and; C) sulphate uptake over time.

reality occur in an open system. In an open system a significant proportion of the Ra may not co-precipitate with the barite once discharged and exist in the aqueous (as the mobile Ra^{2+} ion), or sorbed phases (e.g. adsorbed to sediment particulates) (Landa and Reid, 1983; Van Sice et al., 2018; McDevitt et al., 2019). The amount of radium uptake into the strontiobarite phase can also vary with mixing times, discharge rates and density of produced water solutions; however, the exact nature of this relationship is not clear from this study. Overall, we can confirm that in shallow water environments, radiostrontiobarite co-precipitation and deposition occurs due to the lack of dispersion and/or rapid deposition to the sediment. This is in contrast to deep water environments where production waters are discharged near/at surface and presumably dispersion occurs, resulting in no clear radiological signature in surrounding sediments and waters (Jerez Vegueria et al., 2002; Eriksen et al., 2006; Gafvert et al., 2007; Olsvik et al., 2012). The environmental setting of the receiving environment (e.g. shallow marine or deep sea), its characteristics (e.g. fresh or salt water), and

its corresponding tidal regimes are therefore fundamental factors which need to be considered to better understand the attenuation, impact and fate of radium in the water column. This is key as such factors vary globally between installations as shown from other studies (Landa and Reid., 1983; Pardue and Guo., 1998; Jerez Vegueria et al., 2002; Van Sice et al., 2018; McDevitt et al., 2019).

Due to radiostrontiobarite particulates settling to the sea bed via deposition into shallow water depths, further research into the cumulative effect and fate of such solid phase in a marine environment needs to be conducted to consider the long-term environmental impact of radium in barite. The identification of pyrite as a product of sulphate reduction in these near-shore sediments suggests further studies to underpin assessments of the environmental risk and fate of radium as biogeochemical conditions alter.

Author contributions

F. Ahmad Principal author; all laboratory work; all data analysis and sample preparation and characterisation – (visualisation, conceptualisation, methodology, writing original draft, data curation). K. Morris Input to experimental concept; aided with data interpretation; extensive manuscript review pre- and post-submission - (writing review and editing, supervision). G. T.W. Law Aided with gamma spectroscopy analysis and liquid scintillation counting – (data curation, resources). K. Taylor Project supervisor; input into project concepts and reviewed the manuscript - (writing review and editing, supervision). S. Shaw Principal supervisor; input to experimental concept; aided with data interpretation; extensive manuscript review pre- and post-submission; aided with XAS data collection - (writing review and editing, supervision).

Declaration of competing interest

The authors declare that they have no known competing financial interests or personal relationships that could have appeared to influence the work reported in this paper.

Acknowledgements

The work contained in this paper was conducted during a PhD study undertaken as part of the Natural Environment Research Council (NERC) Centre for Doctoral Training (CDT) in Oil & Gas [grant number [NE/M00578X/1] under its Environmental Impact and Regulation research theme. It was sponsored via a scholarship provided by University of Manchester (UoM), Env Rad Net and the NERC CDT studentship whose support is gratefully acknowledged. We thank Diamond Light Source for access to B18 provided by beam-time award SP17243.

Appendix A. Supplementary data

Supplementary data to this article can be found online at https://doi.org/10.1016/j.chemosphere.2021.129550.

References

Adler, H.H., Kerr, P.F., 1965. Variations in infrared spectra, molecular symmetry and site symmetry of sulfate minerals. Am. Mineral. 50, 132–147. https://doi.org/10.3389/fnhum.2015.00216.

Al-Masri, M.S., Aba, A., 2005. 'Distribution of scales containing NORM in different oilfields equipment', *Applied Radiation and Isotopes*. United Kingdom 63 (4), 457–463, 101016/japradiso200505050.

Averyt, K.B., Paytan, A., Li, G., 2003. A precise, high-throughput method for determining Sr/Ca, Sr/Ba, and Ca/Ba ratios in marine barite. G-cubed 4 (4), 1–10. https://doi.org/10.1029/2002GC000467.

Badr Merdhah, A., Azam, A., Yassin, M., 2008. Study of scale formation due to incompatible water. Jurnal Teknologi 49, 9–26.

Bakke, T., Klungsøyr, J., Sanni, S., 2013. Environmental impacts of produced water and drilling waste discharges from the Norwegian offshore petroleum industry. Mar. Environ. Res. 92, 154–169. https://doi.org/10.1016/j.marenvres.2013.09.012.

Baldi, F., Pepi, M., Burrini, D., Kniewald, G., Scali, D., Lanciotti, E., 1996. Dissolution of barium from barite in sewage sludges and cultures of Desulfovibrio desulfuricans. Appl. Environ. Microbiol. 62 (7), 2398–2404.

Beneš, P., Sedlacek, J., Sebesta, F., Sandrik, R., John, J., 1981. Method of selective dissolution for characterization of particulate forms of Radium and Barium in natural and waste waters. Water Res. 15 (12), 1299–1304. https://doi.org/10.1016/0043-1354(81)90002-6.

Bolze, C.E., Malone, P.G., Smith, M.J., 1974. Microbial mobilization of barite. Chem. Geol. 13 (2), 141–143. https://doi.org/10.1016/0009-2541(74)90006-0.

Candeias, J.P., de Oliveira, D.F., dos Anjos, M.J., Lopes, R.T., 2014. Scale analysis using X-ray microfluorescence and computed radiography. Radiat. Phys. Chem. 95, 408–411. https://doi.org/10.1016/j.radphyschem.2013.03.007.

Ceccarello, S., Black, S., Read, D., Hodson, M.E., 2004. Industrial radioactive barite scale: suppression of radium uptake by introduction of competing ions. Miner. Eng. 17 (2), 323–330. https://doi.org/10.1016/j.mineng.2003.11.007.

Doerner, H.A., Hoskins, W.M., 1925. Co-precipitation of radium and barium sulphates. Journal of the American Chemical Society. American Chemical Society 47 (3), 662–675. https://doi.org/10.1021/ja01680a010.

Dowdall, M., Lepland, A., 2012. 'Elevated levels of radium-226 and radium-228 in marine sediments of the Norwegian Trench ("Norskrenna") and Skagerrak'. Mar. Pollut. Bull. 64 (10), 2069–2076. https://doi.org/10.1016/j.marpolbul.2012.07.022.

Doyi, I., Essumang, D.K., Dampare, S., Glover, E.T., 2016. Technologically enhanced naturally occurring radioactive materials (tenorm) in the oil and gas industry: a review. Rev. Environ. Contam. Toxicol. 238, 107–119. https://doi.org/10.1007/398_2015_5005.

Environment Agency, Food Standards Agency, Food Standards Scotlands, 2015. Natural Resources Wales. Northern Ireland Environment Agency and Scottish Environment Protection Agency. 'Radioactivity in Food and the Environment, 2015', RIFE 21.

Eriksen, D., Sidhu, R., Stralberg, E., Iden, K.I., Hylland, K., Ruus, A., Royset, O., Royset, M.H.G., Rye, H., 2006. Radionuclides in produced water from Norwegian oil and gas installations - concentrations and bioavailability. Czech. J. Phys. 56 (4), 43–48. https://doi.org/10.1007/s10582-006-0486-7.

European Commision, 2014. European Commission, Council Directive 2013/59/Euratom of 5 December 2013 Laying Down Basic Safety Standards for Protection against the Dangers Arising from Exposure to Ionising Radiation, and Repealing Directives 89/618/Euratom, 90/641/Euratom, 96/29/Eur, pp. 1–73 (December 1990).

Fakhru'l-Razi, A., Pendashteh, A., Abdullah, L.Q., Biak, R.A.W., Madeaeni, S.S., Abidin, S.S., 2009. Review of technologies for oil and gas produced water treatment. J. Hazard Mater. 170 (2–3), 530–551. https://doi.org/10.1016/j.jhazmat.2009.05.044.

Fedorak, P.M., Westlake, D.W., Anders, C., Kratochvil, B., Motkosky, N., Anderson, W.B., Huck, P.W., 1986. Microbial release of $^{226}Ra^{2+}$ from (Ba,Ra)SO_4 sludges from uranium mine wastes. Appl. Environ. Microbiol. 52 (2), 262–268.

Fisher, R.S., 1998. Geologic and geochemical controls on naturally occurring radioactive materials (NORM) in produced water from oil, gas, and geothermal operations. Environ. Geosci. 5 (3), 139–150.

Folk, R.L., 2005. Nannobacteria and the formation of framboidal pyrite: textural evidence. Journal of Earth System Science 114 (3), 369–374. https://doi.org/10.1007/BF02702955.

Gafvert, T., Svaeren, I., Gywnn, J., Brungot, A.L., Kolstad, A.K., Lind, B., Alvestad, P., Heldal, H.E., Stralberg, E., Christensen, G.C., Drefvelin, J., Dowdall, M., Rudjord, A.L., 2007. 'Radioactivity in the Marine Environment 2005', Results from the Norwegian Marine Monitoring Programme (RAME). StralevernRapport 2007:10. Ostera Norwegian Radiation Protection Authority, p. 42, 2007 ISBN 0804-4910.

Garner, J., Cairns, J., Read, D., 2015. 'NORM in the East Midlands' oil and gas producing region of the UK'. J. Environ. Radioact. 150, 49–56. https://doi.org/10.1016/j.jenvrad.2015.07.016.

Gonneea, M.E., Paytan, A., 2006. Phase associations of barium in marine sediments. Mar. Chem. 100 (1–2), 124–135. https://doi.org/10.1016/j.marchem.2005.12.003.

Gordon, L., Rowley, K., 1957. 'Coprecipitation of radium with barium sulfate', *analytical chemistry*. American Chemical Society 29 (1), 34–37. https://doi.org/10.1021/ac60121a012.

Grung, M., Ruus, A., Holth, T.F., Sidhu, R.S., Eriksen, D.O., Hylland, K., 2009. Bioaccumulation and lack of oxidative stress response in the ragworm *H. diversicolor* following exposure to ^{226}Ra in sediment. J. Environ. Radioact. 100 (5), 429–434. https://doi.org/10.1016/j.jenvrad.2009.03.001.

Hedström, H., Persson, I., Skarnemark, G., Ekberg, C., 2013. Characterization of radium sulphate. Journal of Nuclear Chemistry 2013, 1–4. https://doi.org/10.1155/2013/940701.

Holdway, D.A., 2002. The acute and chronic effects of wastes associated with offshore oil and gas production on temperate and tropical marine ecological processes. Mar. Pollut. Bull. 44 (3), 185–203. https://doi.org/10.1016/S0025-326X(01)00197-7.

Hosseini, A., Beresford, N.A., Brown, J.E., Jones, D.G., Phaneauf, M., Thorring, H., Yankovich, T., 2010. Background dose-rates to reference animals and plants

arising from exposure to naturally occurring radionuclides in aquatic environments. J. Radiol. Prot. 30 (2), 235–264. https://doi.org/10.1088/0952-4746/30/2/S03.

Hunt, J.M., 1979. Petroleum Geochemistry and Geology - A Series of Books in Geology. W. H. Freeman and Company, San Francisco, ISBN 0716710056, p. 617.

IAEA, 2004. Radiation protection and the management of radioactive waste in the oil and gas industry. Environ. Health Perspect. 34 (34), 130.

ICRP, 2007. ICRP Publication 103 the 2007 Recommendations of the International Commission on Radiological Protection.

IOGP, 2016. Managing Naturally Occurring Radioactive Material (NORM) in the Oil and Gas Industry, vol. 412. International Association of Oil & Gas Producers, p. 68. March.

Jacobs, R.P.W.M., Grant, R.O.H., Kwant, J., Marquenie, J.M., Mentzer, E., 1992. The composition of produced water from shell operated oil and gas production in the North sea - produced water: technological/environmental issues and solutions. In: Ray, J.P., Engelhardt, F.R. (Eds.). Springer US, Boston, MA, pp. 13–21. https://doi.org/10.1007/978-1-4615-2902-6_2.

Jerez Vegueria, S.F., Godoy, J.M., Miekeley, N., 2002. Environmental impact studies of barium and radium discharges by produced waters from the "Bacia de Campos" oil-field offshore platforms, Brazil. J. Environ. Radioact. 62 (1), 29–38. https://doi.org/10.1016/S0265-931X(01)00148-5.

Keith-Roach, M.J., 2002. Interactions of microorganisms with radionuclides. In: Keith-Roach, M.J., Livens, F.R. (Eds.), 2. Elsevier, Amsterdam, ISBN 9780080534909, pp. 61–100 (Radioactivity in the environment).

Landa, E.R., Reid, D.F., 1983. Sorption of radium-226 from oil-production brine by sediments and soils. Environ. Geol. 5 (1), 1–8. https://doi.org/10.1007/BF02381293.

Luptáková, A., Kotulicova, I., Balintova, M., Demcak, S., 2015. Bacterial reduction of barium sulphate by sulphate-reducing bacteria. Nova Biotechnologica et Chimica 14 (2), 135–140. https://doi.org/10.1515/nbec-2015-0022.

McDevitt, B., McLaughlin, M., Cravotta, C.A., Ajemigbitse, M.A., Van Sice, K.J., Blotevogel, J., Borch, T., Warner, N.R., 2019. Emerging investigator series: radium accumulation in carbonate river sediments at oil and gas produced water discharges: implications for beneficial use as disposal management. Environ. Sci.: Processes & Impacts. The Royal Society of Chemistry. https://doi.org/10.1039/C8EM00336J.

Mitchell, R.W., Grist, D.M., Boyle, M.J., 1980. Chemical treatments associated with North Sea projects. J. Petrol. Technol. 32 (5), 904–912. https://doi.org/10.2118/7880-PA.

Neff, J.M., 2002. 'Barium in the Ocean', *Bioaccumulation In Marine Organisms*, pp. 79–87. https://doi.org/10.1016/B978-008043716-3/50005-1 (January).

Olsvik, P.A., Berntssen, M.H.G., Hylland, K., Eriksen, D.O., Holen, E., 2012. Low impact of exposure to environmentally relevant doses of ^{226}Ra in Atlantic cod (*Gadus morhua*) embryonic cells. J. Environ. Radioact. 109, 84–93. https://doi.org/10.1016/j.jenvrad.2012.02.003.

Ouyang, B., Akob, D.M., Dunlap, D., Renock, D., 2017. Microbially mediated barite dissolution in anoxic brines. Appl. Geochem. 76, 51–59. https://doi.org/10.1016/j.apgeochem.2016.11.008.

Pardue, J.H., Guo, T.Z., 1998. Biogeochemistry of ^{226}Ra in contaminated bottom sediments and oilfield waste pits. J. Environ. Radioact. 39 (3), 239–253. https://doi.org/10.1016/S0265-931X(97)00047-7.

Phillips, E.J.P., Landa, E.R., Kraemer, T., Zielinski, R., 2001. Sulfate-reducing bacteria release barium and radium from naturally occurring radioactive material in oilfield barite. Geomicrobiol. J. 18 (2), 167–182. https://doi.org/10.1080/01490450120549.

Proske, U., Wood, R., Fallon, S., Stevenson, J., 2015. Use of heavy liquid density separation to remove pyrite from sediment samples for radiocarbon dating. Quat. Geochronol. 25, 66–71. https://doi.org/10.1016/j.quageo.2014.10.002.

Ramaswamy, V., Vimalathithan, R.M., Ponnusamy, V., 2010. Synthesis and characterization of BaSO4 nano particles using micro emulsion technique. Adv. Appl. Sci. Res. 1 (3), 197–204.

Ravel, B., Newville, M., 2005. ATHENA, artemis, hephaestus: data analysis for X-ray absorption spectroscopy using IFEFFIT. J. Synchrotron Radiat. 12 (4), 537–541. https://doi.org/10.1107/S0909049505012719.

Røe Utvik, T.I., 1999. Chemical characterisation of produced water from four offshore oil production platforms in the North Sea. Chemosphere 39 (15), 2593–2606. https://doi.org/10.1016/S0045-6535(99)00171-X.

Rosenberg, Y.O., Metz, V., Oren, Y., Volkman, Y., Ganor, J., 2011a. a)) 'Co-precipitation of radium in high ionic strength systems: 2. Kinetic and ionic strength effects'. Geochem. Cosmochim. Acta 75 (19), 5403–5422. https://doi.org/10.1016/j.gca.2011.07.013.

Rosenberg, Y.O., Metz, V., Ganor, J., 2011b. b)) 'Co-precipitation of radium in high ionic strength systems: 1. Thermodynamic properties of the Na–Ra–Cl–SO_4–H_2O system – estimating Pitzer parameters for RaCl2'. Geochem. Cosmochim. Acta 75 (19), 5389–5402. https://doi.org/10.1016/j.gca.2011.06.042.

Rosenberg, Y.O., Sadeh, Y., Metz, V., Pina, C.M., Ganor, J., 2014. 'Nucleation and growth kinetics of $Ra_xBa_{1-x}SO_4$ solid solution in NaCl aqueous solutions'. Geochem. Cosmochim. Acta 125, 290–307. https://doi.org/10.1016/j.gca.2013.09.041.

Roychoudhury, A.N., Kostka, J.E., Van Cappellen, P., 2003. 'Pyritization: a palaeoenvironmental and redox proxy reevaluated', *Estuarine*. Coastal and Shelf Science 57 (5–6), 1183–1193. https://doi.org/10.1016/S0272-7714(03)00058-1.

Schlanger, S.O., 1988. Strontium storage and release during depostion and diagenesis of marine carbonates related to sea-level variation. In: Lerman, A., Maybeck, M. (Eds.), Physical and Chemical Weathering in Geochemical Cycles. NATO ASI Series (Series C: Mathmatical and Physcial Sciences), vol. 251. Springer, Dordrecht, pp. 323–329. https://doi.org/10.1007/978-94-009-3071-1_15.

Siddeeg, S.M., Bryan, N.D., Livens, F.R., 2015. 'Behaviour and mobility of U and Ra in sediments near an abandoned uranium mine, Cornwall, UK', *Environmental Science: processes & Impacts*. The Royal Society of Chemistry 17 (1), 235–245. https://doi.org/10.1039/C4EM00230J.

Stevenson, A.G., Tait, B.A.R., Richardson, A.E., Smith, T., Nicolson, R.A., Stewart, H.R., 1995. The Geochemistry of Seabed Sediments of the United Kingdom Continental Shelf; the North Sea, Hebrides and West Shetland Shelves, and the Malin-Hebrides Sea Area. British Geological Survey Technical Report, p. 484 (WB/95/028) (unpublished).

Todd, A.C., Yuan, M., 1990. Barium and strontium sulfate solid solution formation in relation to North Sea scaling problems. SPE Production Engineering. Society of Petroleum Engineers 5 (3), 279–285. https://doi.org/10.2118/18200-PA.

Todd, A.C., Yuan, M.D., 1992. Barium and strontium sulfate solid-solution scale formation at elevated temperatures. SPE Production Engineering. Society of Petroleum Engineers 7 (1), 85–92. https://doi.org/10.2118/19762-PA.

Tokunaga, K., Kozai, N., Takahashi, Y., 2018. A new technique for removing strontium from seawater by coprecipitation with barite. J. Hazard Mater. 359, 307–315. https://doi.org/10.1016/j.jhazmat.2018.07.044.

VanLoon, G.W., 2000. Environmental chemistry: a global perspective. In: Duffy, S.J. (Ed.). Oxford University Press, New York, Oxford, ISBN 0198564406, p. 560.

Van Sice, K., Cravotta, C.A., McDevitt, B., Tasker, T.L., Landis, J.D., Puhr, J., Warner, N.R., 2018. Radium attenuation and mobilization in stream sediments following oil and gas wastewater disposal in western Pennsylvania. Appl. Geochem. 98, 393–403. https://doi.org/10.1016/j.apgeochem.2018.10.011.

Vinograd, V.L., Kulik, D.A., Brandt, F., Klinkenberg, M., Weber, J., Winkler, B., Bosbach, D., 2018. Thermodynamics of the solid solution - aqueous solution system (Ba,Sr,Ra)SO4 + H2O: I. The effect of strontium content on radium uptake by barite. Appl. Geochem. 89, 59–74. https://doi.org/10.1016/j.apgeochem.2017.11.009.

Wilkins, M.J., Vaughan, D.J., Beadle, I., Livens, F.R., 2007. The influence of microbial redox cycling on radionuclide mobility in the subsurface at a low-level radioactive waste storage site. Geobiology 5 (3), 293–301. https://doi.org/10.1111/j.1472-4669.2007.00101.x. John Wiley & Sons, Ltd (10.1111),.

Yuan, M., Todd, A.C., Sorbie, K.S., 1994. Sulphate scale precipitation arising from seawater injection: a prediction study. Mar. Petrol. Geol. 11 (1), 24–30. https://doi.org/10.1016/0264-8172(94)90006-X.

Zeissler, C.J., Lindstrom, R.M., McKinley, J.P., 2001. Radioactive particle analysis by digital autoradiography. J. Radioanal. Nucl. Chem. 248 (2), 407–412. https://doi.org/10.1023/A:1010640411441.

Zhang, T., Gregory, K., Hammack, R.W., Vidic, R.D., 2014. 'Co-precipitation of radium with barium and strontium sulfate and its impact on the fate of radium during treatment of produced water from unconventional gas extraction', *environmental science & technology*. American Chemical Society 48 (8), 4596–4603. https://doi.org/10.1021/es405168b.